Identification of insulating materials thermal properties by inverse method using reduced order model

Ana Gabriela Chavez Castillo, Benjamin Gaume, Y. Rouizi, O. Quéméner, Patrick Glouannec

Identification of insulating materials thermal properties by inverse method using reduced order model

A.G. Chavez Castillo[a], B. Gaume[a], Y. Rouizi[a,*], O. Quéméner[a], P. Glouannec[b]

[a] *Université Paris-Saclay, Univ Evry, LMEE, 91020, Evry, France.*
[b] *Institut de Recherche Dupuy de Lôme, Université Bretagne Sud, 56321 Lorient Cedex, France.*

Abstract

The analytical models used by hot-wire type probes are no longer suitable for the characterization of insulating materials. This paper proposes a solution, which is based on a numerical reduced order technique named AROMM (Amalgamated Reduced Order Modal Method) coupled to an inverse procedure. We demonstrate that a single reduced order model provides precise results for insulated materials characterized by different thermal properties, with the advantage of computing 250 times faster than a classical finite element modelization. Such model is then tested through multiple scenarios in order to evaluate the accuracy of the proposed methodology. Results show the importance of the sensitivity of the measurement regarding the sought parameters, which later intervene during the identification process. A statistical study allows us to access a satisfying confidence interval for a common measurement noise. At last, a study on the influence of an eventual thermal contact resistance is conducted.

Keywords:
Reduced model; Branch eigenmodes reduction method; inverse problem; thermal characterization; thermal properties; insulating materials; thermal contact resistance.

*Corresponding author. Tel.:+33 1 69 47 79 36
Email address: yassine.rouizi@univ-evry.fr (Y. Rouizi)

Preprint submitted to International Journal of Heat and Mass TransferSeptember 17, 2020

1. INTRODUCTION

Nowadays, environmental constraints are increasing at a fast rate, leading to the appearance of new materials in the building world, in particular thermal insulators.

However, their use stays limited due to non-availability of databases in reference to their intrinsic properties. Moreover, we lack hindsight regarding their sustainability (humidity sensitivity, fluctuation of micro-structure, fungal growth).

The purpose of this paper is to present a method which enables to identify on site thermal properties of insulating materials, in order to maintain an active monitoring of their properties overtime.

In literature, some characterization methods exist :

- The most simple techniques which enable to determine an isotropic conductivity $k\,[\mathrm{W.m^{-1}K^{-1}}]$ in equilibrium is the hot plate method [1]. Jannot *et al.* [2] created a three-layer device combined with an inverse method aimed at improving the precision on the estimated values specifically for very low conductivity materials ($k < 0.15$ W.m^{-2}.K^{-1}). It is often coupled with a DSC calorimetric technique to determine the heat capacity $Cp\,[\mathrm{J.\ kg^{-1}.K^{-1}}]$ or $c\,[\mathrm{J.\ m^{-3}.K^{-1}}]$.

- Another technique widely used in the laboratory is the flash method [3, 4, 5]. Initially developed to measure diffusivity $a = \frac{k}{c}\ [m^2/s]$, the analytical relations of integral transforms type allow by inverse method to go back quickly to the two parameters k and c [6, 7, 8]. This experimental principle has also made it possible to use numerical models to determine non-homogeneous properties: Brouns *et al.* [9] relied on surface temperature measurements by infrared thermography, paired with a Finite Element Method (FEM) to evaluate the thermal conductivity of a specimen and find the presence of a faulty area. Reulet *et al.* [10] applied a numerical conduction model linked to the iterative method of Levenberg-Marquardt to estimate simultaneously the set of thermal properties $\{Cp,\ k_{xx},\ k_{yy},k_{zz}\}$ of an orthotropic sample. Adamczyk *et al.* performed several studies ([11, 12]) based on the flash method with the purpose of measuring thermal conductivities on isotropic and orthotropic materials.

- Flat shock probes, of which the best known is the HotDisc®[13, 6], allow here again by inverse method the determination of the 2 parameters

k and c. Raji *et al.* [14] characterized a wall made of stacked laminated solid-wood planks by implementing a thermal effusivity relation in the analytical equations of the hot strip method for both directions of the fiber (perpendicular and parallel). The results pointed out that thermal properties of wood depend greatly on the water content inside the wood fiber, as well as the important role that permeability and the diffusion coefficient could have.
Lagüela *et al.* [15] provided a theoretical derivation of the hot-disc method to obtain the thermal diffusivity and conductivity in anisotropic materials, specifically in their case for wood.

Searching for a easier way to characterize insulating materials, Jannot *et al.* [16] developed a simplified estimation method based on the hot-plate method by using a 1.2 cm wide hot-strip and a thermocouple. They then deducted simultaneously the effusivity and conductivity from a temperature recording by using a linear regression of the heat equation.

A major inconvenience with most of these techniques is that they are essentially used in laboratory : Even if the flash method has been tested in situ (Kruczek *et al.* [17]), the difficulties are numerous: the profile of the laser source that creates the heating must be precisely known. In addition, given the relatively large and fragile equipment, this technique is not well suited to frequent travel. Finally, even if recent work proposes to go back to multilayer characteristics [18], the characterization of a sandwiched insulating material seems to be difficult. As far as the HotDisc is concerned, its principle is not adapted to an in situ measurement and moreover, even if its major interest is its experimental simplicity, a major defect remains: its fragility.

Another technologie it's the "hot wire or needle probe method", which consists of an infinite line source with constant power per unit length, placed inside an infinite medium, having a thermocouple to record the temperature transient evolution at an x distance. From the point of view of the experimental protocol, this solution meets the specifications, since the equipment is light, easily transportable, requiring a moderate measurement time, and inexpensive.

Initially intended to determine the conductivity from more or less simple analytical laws (Jeager [19], Blackwell [20]), it has been used in many fields [21, 22, 23]. For all these models, the resulting plot of the temperature

evolution against the natural logarithm of time is characterized by a linear zone, for which the slope gives direct access to the thermal conductivity value. In addition, the use of inverse techniques also allows, as for the other techniques, to go back to the 2 parameters simultaneously k and c, always based on analytical laws [24, 25].

But at the same time, studies are questioning the validity of these models for materials with low conductivity [26, 27, 28, 29]. For these authors, the analytical model presents a limitation for the characterization of insulating materials even if it is used in an inverse procedure. This is due to a strong simplification because the model does not allow to take into account the inertia of the probe, the non homogeneity of temperature, and the heat flows that exist along the sensor. This phenomena, often negligible with a conductive sample, must be taken into account in the case of insulation. This is why numerical models have been developed. Given the limits of the number of degrees of freedom of the numerical models that can be applied in an inverse method, all models have so far been simulated only in 2D axisymmetric, considering the probe perfectly homogeneous and dissipating a uniform power density [28, 30].

In this paper, our goal is to use a numerical model associated to an inverse procedure, in order to broaden the application of a classical heat-wire type probe which could be used in situ for an highly insulating materials, in order to determine their thermal conductivity and thermal volumetric capacity.To overcome the numerical difficulty caused by the large number of degrees of freedom of the model, incompatible with the iterative inverse procedure, a reduced modal model is used instead. The challenge lies then in establishing one single reduced model suitable to a variety of values of thermal properties of the insulating materials. Therefore, we seek to show the effectiveness of such procedure.

The first part of this paper introduces the geometry of an existing hot-wire probe and the conditions affecting the material to be studied. The construction of a numerical model is conducted as well. We then move on to the use of a modal reduction method, where the previously numerical model is reduced; thus showing the capacity of the method. Section 4 addresses the inverse procedure. It thoroughly explains each of the stages taken in order to conduct an identification, and presents the results obtained for the study. And finally, conclusions and perspectives are discussed.

2. PHYSICAL PROBLEM

2.1. Studied configuration

Here we consider Ω_I as one portion of a slab of insulating material (Figure 1) whose thermal conductivity k_I [W.m^{-1}.K^{-1}] and capacity c_I [J.m^{-3}.K^{-1}] are to be determined. This insulator is shaped like a cube, where each side measures 10 cm.

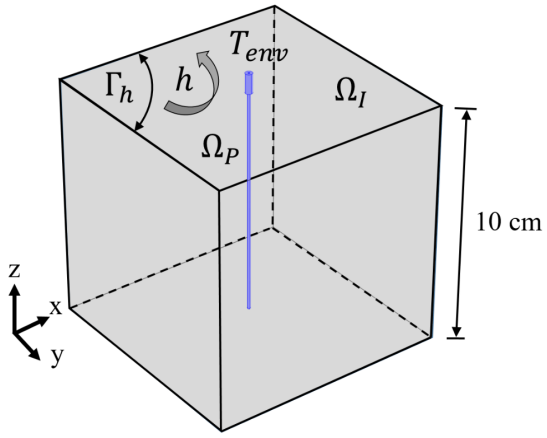

Figure 1: Studied system

The system uses an existing hot-wire probe Ω_P, developped in a laboratory, composed by a heating wire and two thermocouples initially conceived to identify solely thermal conductivities. They are embedded in a steel needle-like body filled with glue (Figure 2). This probe is particularly thin, since its diameter is $D = \mathbf{2}$ mm for a length $L = \mathbf{9.3}$ cm .

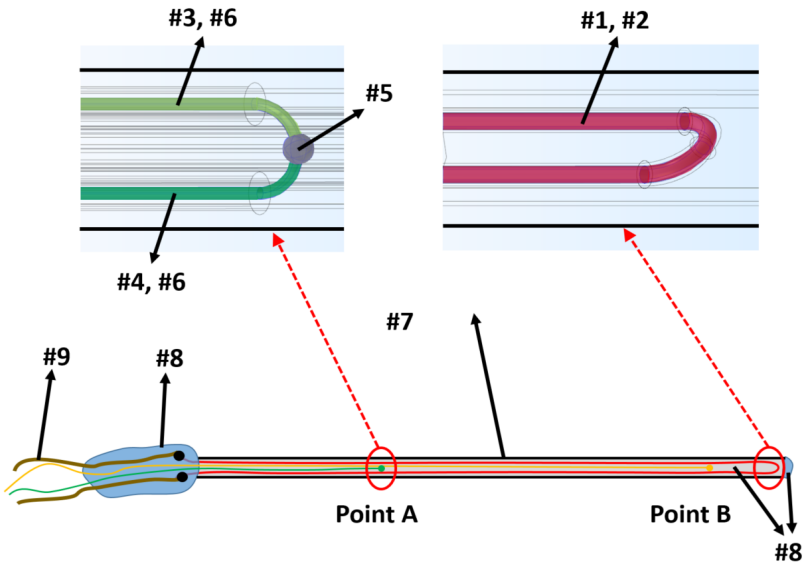

Figure 2: Geometry of the studied system

This probe Ω_P is composed of different materials, whose thermal conductivities (k_i) and volumetric thermal capacities (c_i) are presented on Table 1.

No. of domain in Ω_P	k_{P_i} [W.m^{-1}.K^{-1}]	c_{P_i} [J.m^{-3}.K^{-1}]
#1 - Ω_{HW} Heating wire	19.5	3.47×10^6
#2 - Ω_{HS} Heating wire sheath	0.25	2.25×10^6
#3 - Ω_{Ch} Chromel	19	3.81×10^6
#4 - Ω_A Alumel	29.7	4.50×10^6
#5 - Ω_{Th} Thermocouple	24.35	4.15×10^6
#6 - Ω_{ThS} Thermocouple sheath	0.2	2.25×10^6
#7 - Ω_S Steel	16.3	3.97×10^6
#8 - Ω_G Glue/filling	0.1	3.15×10^5
#9 - Ω_C Copper	390	3.38×10^6

Table 1: Physical parameters of the hot-wire probe

The insulating materials (Ω_I) will undergo a convective condition on the side (Γ_h) where the probe (Ω_P) is inserted and which is characterized by a convective coefficient $h = 10$ [W.m^{-2}.K^{-1}] and an environmental temperature $T_{env} = 0$ [°C] (temperature elevation). Starting from an uniform initial temperature $T_0 = 0$ [°C], the heating wire Ω_{HW} will dissipate a known power $\pi = 0.06$ $[W]$. All other surfaces (noted Γ_0) are insulated. This thermal problem is described by the following equations (with $\Omega = \Omega_I \cup \Omega_P$)

$$\begin{cases} \forall M \in \Omega\,,\, t > 0 & c\dfrac{\partial T}{\partial t} = \overrightarrow{\nabla}(k\overrightarrow{\nabla}T) + \Pi \\ \forall M \in \Gamma_h\,,\, t > 0 & k\overrightarrow{\nabla}T.\overrightarrow{n} = -hT \\ \forall M \in \Gamma_0\,,\, t > 0 & \overrightarrow{\nabla}T.\overrightarrow{n} = 0 \\ \forall M \in \Omega\,,\, t = 0 & T = T_0 = 0 \end{cases} \tag{1}$$

where:

- k and c gather all the values of thermal conductivities and heat capacities, including those regarding the probe and the insulating material,
- and Π is equal to π in the heating wire Ω_{HW} and zero elsewhere.

The main goal will be to seek the values of the thermal properties of the insulating material, being the thermal conductivity k_I and the volumetric heat capacity c_I. This is achieved by previously knowing the materials conforming the probe, as well as the thermal loads that the insulator will undergo.

2.2. Numerical model

The resolution of the problem defined by Eq.(1) is done from its variational formulation, in which the test function f $\in H^1(\Omega)$ is defined:

$$\int_\Omega c\frac{\mathrm{d}T}{\mathrm{d}t} f d\Omega = -\int_\Omega k\vec{\nabla}T \cdot \vec{\nabla} f d\Omega \; - \int_{\Gamma_h} hTf d\Gamma + \int_\Omega \Pi f d\Omega \tag{2}$$

By expressing each of the preceding volume integrals as a sum of two terms, on the one hand as the volume of the probe Ω_P and on the other hand, as that of the insulating material Ω_I, it is possible to isolate the unknown sought terms, that is to say, the thermal conductivity k_I and the heat capacity c_I of the insulator:

$$c_I \int_{\Omega_I} \frac{\mathrm{d}T}{\mathrm{d}t} f \, d\Omega + \int_{\Omega_P} c_P \frac{\mathrm{d}T}{\mathrm{d}t} f \, d\Omega = -k_I \int_{\Omega_I} \vec{\nabla} T \cdot \vec{\nabla} f \, d\Omega \\ - \int_{\Omega_P} \vec{\nabla} T \cdot k_P \vec{\nabla} f \, d\Omega - \int_{\Gamma_h} h \, T \, f \, d\Gamma + \int_{\Omega_{HW}} \pi \, f \, d\Omega \tag{3}$$

Once a spatial discretisation is performed by the Finite Element Method (FEM), considering a linear interpolation law (type P1 elements), we obtain the following matrix expression (respecting the same order as in Eq.(3)):

$$(c_I \mathbf{C_I} + \mathbf{C_P}) \dot{\mathbf{T}} = (k_I \mathbf{K_I} + \mathbf{A}) \mathbf{T} + \mathbf{U} \tag{4}$$

The size of these matrices are $[N,\ N]$, where $N = 61,591$ taking into consideration the degree of precision for the representation of the geometry.

A numerical simulation was executed, using a second-order solver working at a variable time-step, to evaluate the temperature field of the formerly discussed insulator. With the same set of thermal characteristics ($k_I = 0.041$ [W.m^{-1}.K^{-1}] and $c_I = 1.15 \times 10^5$ [J.m^{-3}.K^{-1}]). Our simulation has been validated with the modeling software COMSOL Multiphysics®.

Figure 3 shows the evolution of the temperature at the 2 measuring points A and B of the probe over time, as well as the results obtained by the Blackwell analytical model. One can thus note the important difference between these two models. In addition, the inexistence of a linear law as a function of the logarithm of time in the case of the numerical model. It is thus this one which must be used in the case of the identification of an insulating material.

Figure 4 shows the numerical temperature profiles at both measuring points A and B of the probe. Depending on the axis orientation, the temperature profile changes. There is a presence of a notable non-homogeneity regarding the temperature inside the probe, both radially (concerning the heating wire), as well as longitudinally (thermal flow along the probe). The difference in temperature ΔT equals to 0.56 [°C]. This proves how essential it is to know the probe's geometry and thermal properties with precision, and not just simply consider it as an uniform object englobing all components. We note that ΔT could vary according to the insulating material being tested, and in case of a lower conductivity, the gap in temperature between both measuring points will become more noticeable.

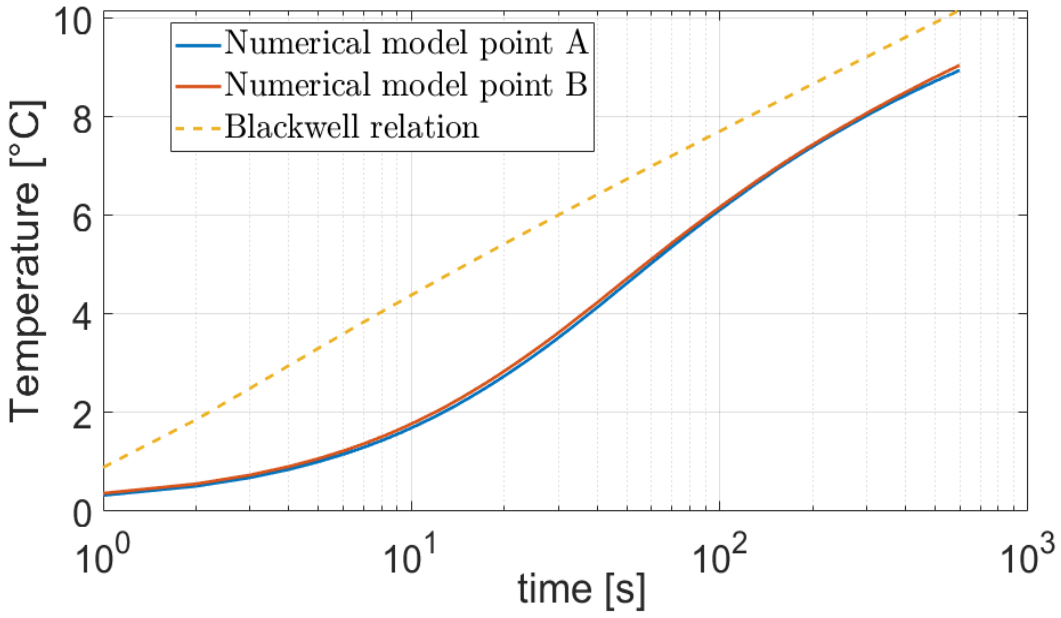

Figure 3: Temperature evolution : analytical and numerical models

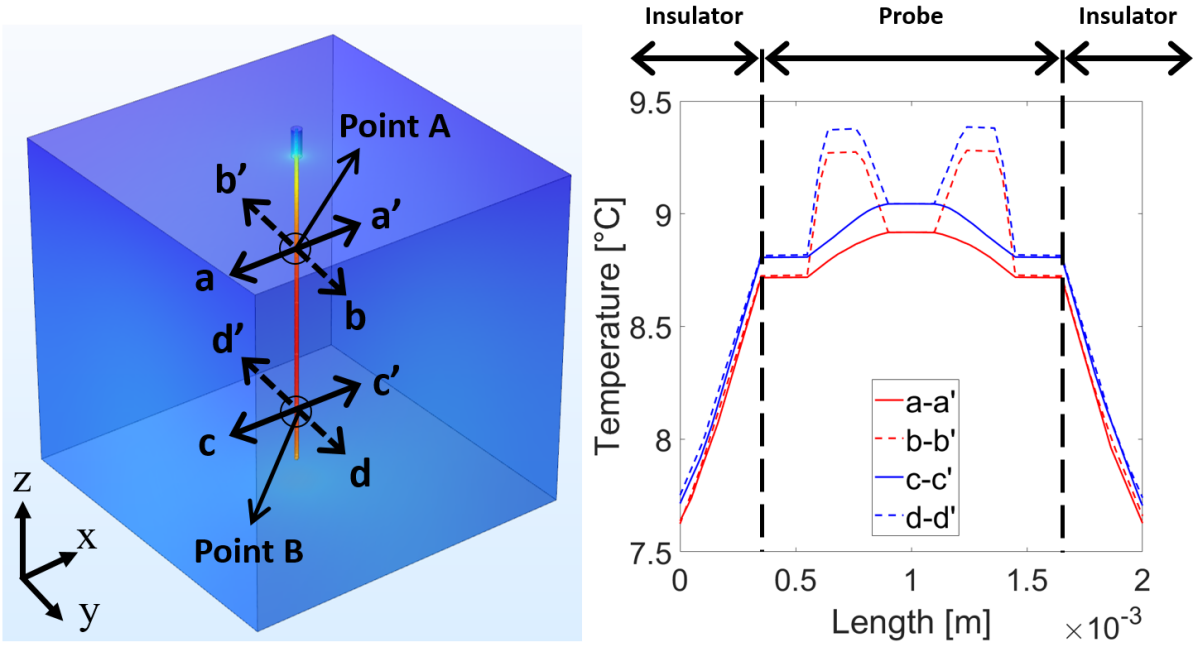

Figure 4: Temperature profiles at $t = 600$ [s]

For the rest of the study, this numerical model called complete model will be used for 2 things:

- It will make it possible to obtain virtual measurements at the results obtained at measurement points A and B, by adding Gaussian noise: of zero mean, constant standard deviation and uncorrelated along time.
- As will be shown in the following, it will serve as a starting point for the construction of an accurate model for the whole range of insulators that we wish to characterize with this probe.

3. Modal reduction

3.1. General principle of modal reduction

The modal reduction method is based on the decomposition of the temperature field into a small number $\tilde{n}$ of known spatial functions $\tilde{V}_i(M)$ called eigenmodes. We are then able to approximate the sought temperature $\tilde{T}(M,t)$, defined as:

$$T(M,t) \simeq \tilde{T}(M,t) = \sum_{i=1}^{\tilde{n}<<N} \tilde{x}_i(t)\tilde{V}_i(M) \tag{5}$$

where $\tilde{x}_i$ are the unknown excitation states of the eigenmodes $\tilde{V}_i(M)$.

Based on this principle, different techniques exist, such as the Modal Identification Method (MIM) [31, 32], the Proper Generalized Decomposition (PGD) [33], and the most well-known the Proper Orthogonal Decomposition (POD) [34, 35],

For this study, we chose to apply another method called the Amalgam Reduction Order Modal Model (AROMM) method. Initiated by Neveu *et al.* [36], this technique is adapted to problems with variable parameters, and has so far been used for problems of identification of sources or heat flows [37, 38, 39, 40]. The main difference between POD and AROMM is the way in which eigenvectors are obtained $\tilde{V}_i$: Both techniques use several reference temperature fields, the POD makes a statistical treatment of them by using a spatial autocorrelation function, while the AROMM method uses the heat equation to calculate a large generic initial base, which is then reduced from the reference cases according to a minimization process.

Very few studies have used these different modal reduction techniques for the identification of the conductivity of materials: Adamczyk [41] uses a POD type model, et Girault [42] develops the MIM technique.

The following paragraphs specify the different steps in the construction of the modal reduced base using the AROMM method.

3.2. The complete base of the AROMM method

The complete basis is obtained by the resolution of a particular eigenvalues problem which takes up the operators associated with the heat equation (eq 1) :

$$\begin{cases} \forall M \in \Omega \quad , \quad k_0 \overrightarrow{\nabla}.(\overrightarrow{\nabla}\widehat{V}_i) = z_i \, c_0 \, \widehat{V}_i \\ \forall M \in \Gamma_h \quad , \quad k_0 \overrightarrow{\nabla}\widehat{V}_i.\overrightarrow{n} = -z_i \, \zeta \, \widehat{V}_i \end{cases} \tag{6}$$

The feature of this problem is that the eigenvalues z_i are present in the boundaries condition. The variational form of (6) is written, separating the domain of the probe Ω_P from that of the insulator Ω_I :

$$\begin{aligned} -\int_{\Omega_I} \vec{\nabla} V_i \cdot k_{I_0} \vec{\nabla} f \, d\Omega - \int_{\Omega_P} \vec{\nabla} V_i \cdot k_{P_0} \vec{\nabla} f \, d\Omega = \\ z_i \left(\int_{\Omega_I} V_i \, c_{I_0} \, f \, d\Omega \; + \int_{\Omega_P} V_i \, c_{P_0} \, f \, d\Omega + \int_{\Gamma_h} \zeta \, f \, V_i \, d\Gamma \right) \end{aligned} \tag{7}$$

The choice of unique values for the different parameters involved in this eigenvalue problem is as follows:

- The probe domain corresponding to Ω_P had every single one of its components with a certain well-known thermal property. The properties k_{P_0} and c_{P_0} of the different elements of the probe correspond to the known real values (table 1).

- With respect to the insulator for which there is no fixed value in the heat equation (3) the value of the parameters k_I and c_I, we opted here for an arbitrary value, near to the range of the materials being studied:

$$\forall M \in \Omega_I \, , \quad k_{I_0} = 0.01 \, [\mathrm{W.m^{-1}.K^{-1}}] \, , \quad c_{I_0} = 10000 \, [\mathrm{J.m^{-3}.K^{-1}}] \tag{8}$$

- The quantity ζ $[\mathrm{J.m^{-2}K^{-1}}]$ is called the Steklov parameter and it is a simple coefficient that allows to maintain the physical dimensions of the quantity in the boundaries condition equations. To balance the two terms linked to the eigenvalue in (eq. 7), an appropriate choice of the Steklov coefficient ζ is given by:

$$\zeta \simeq \frac{\displaystyle\int_{\Omega_I} c_{I_0} \, d\Omega \; + \int_{\Omega_P} c_P \, d\Omega}{\displaystyle\int_{\Gamma_h} d\Gamma} = 3528 \, [\mathrm{J.m^{-2}.K^{-1}}] \tag{9}$$

The contribution of these Branch vectors is that they form a basis for all types of thermal problems, whatever the set of values of the thermophysical characteristic of the isolant k_I and c_I:

$$T(M,t)_{(c_I,k_I)} = \sum_{i=1}^{N} x_i(t)\ V_i(M)_{(c_{I_0},k_{I_0},\zeta)} \tag{10}$$

These Branch basis are characterized by the orthogonality property:

$$\forall i,\ j \in \mathbb{N}, \int_{\Omega} V_i\ c_0\ V_j\, d\Omega + \int_{\Gamma} V_i\ \zeta\ V_j\ d\Gamma = \delta_{ij} \tag{11}$$

where δ_{ij} corresponds to the Kronecker function.

The numerical calculations for this Branch basis are achieved by using the Arnoldi Method [43], which allows to calculate the first modes characterized by their smallest value of z_i (absolute value). The whole (100%) base is computed, consisting of 61,591 modes, needing approximately 3 hours and 20 minutes of CPU time on a Dell Precision 7530 with Intel Xeon.

3.3. Basis reduction

The reduction of the complete base calculated in the previous stage can be easily done by removing some modes, according to a criteria that can be time-based [44] or energetic [45]. The method chosen for this study is a more developed technique, known by the name of Amalgam Reduction [46], that is based on a distribution of the eigenmodes space into $\tilde{n}$ subspaces that are orthogonal to each other. Every subspace is conformed by a main mode $V_{j,0}$, and $\tilde{n}_j$ minor modes. The latter will provide additional thermal information to each main mode, by creating a mix of modes, hence the name of the method.

The core of the technique relies in rebuilding new modes $\tilde{V}_j$ by linear combinations of initial modes V_i, with the particularity that each eigenvector is used only once, either as a main mode or as a minor mode:

$$\forall j \in \left\{1, \tilde{n}\right\} \qquad \tilde{V}_j = V_{j,0} + \sum_{p=1}^{\tilde{n}_j} \alpha_{j,p}\, V_{j,p} \tag{12}$$

The distribution of initial modes in the sub-spaces of the amalgamated basis, as well as determining the amalgam coefficients α, are achieved by

minimizing a criteria J_R based on the difference between the temperature fields obtained respectively by the complete model T and the reduced model $\tilde{\text{T}}$. These calculations are then made from known temperature fields, characteristic of the simulated process.

In the case of the insulating material, since we cannot predict the exact set of thermal properties, we are forced to take into account a wider spectrum instead of limiting it to just one set of values. Therefore, we will build a compound scenario where the reference temperature fields $T_{(R_i)}$, $i = [1, ..., 4]$, are derived from simulations presenting different sets of thermal properties. Table 2 presents the selected reference cases for the basis reduction.

No. Reference case	$k_{I_{Ref}}$ $[10^{-2}\text{W.m}^{-1}\text{.K}^{-1}]$	$c_{I_{Ref}}$ $[10^{4}\text{J.m}^{-3}\text{.K}^{-1}]$
R_1	1	1.5
R_2	1	150
R_3	6	1.5
R_4	6	150

Table 2: Amalgam reduction reference points

The criteria J_R is built in order to take advantage of the orthogonality properties of the complete base (Eq.(11)). It leads to a fast and sequential optimization process as a function of the number of modes of the reduced base.

$$J_R = \sum_{i=1}^{4} \int_{\tau} \left[\int_{\Omega} c_0 \left(T_{(R_i)} - \tilde{T}_{(R_i)} \right)^2 d\Omega + \int_{\Gamma} \zeta \left(T_{(R_i)} - \tilde{T}_{(R_i)} \right)^2 d\Gamma \right] dt \quad (13)$$

In order to determine the order of the reduced model used afterwards, the projection of the known temperature fields T on the reduced base $\tilde{V}$ makes it possible, thanks to the orthogonality properties, to obtain the states of excitation of every mode:

$$\tilde{x}_i = \int_{\Omega} \tilde{V}_i \; c_0 \; T d\Omega + \int_{\Gamma} \tilde{V} \; \xi \; T d\Gamma \quad (14)$$

Through Eq.(5) we are able to obtain the states that will allow to determine the integrality of the sought temperature field and then error the

between the complete model and the reconstructed reduced model. For this study, only the measurement points A and B will be considered:

$$P \in [A,\ B], \qquad \epsilon(P,t) = T(P,t) - \sum_{i=1}^{\tilde{n}} \tilde{x}_i(t) \cdot \tilde{V}_i(P) \tag{15}$$

The mean and maximum values of these errors at the two measuring points over the entire duration of the test are then deduced:

$$\begin{cases} P \in [A,\ B], & \epsilon_{max}(P) = \max\limits_{t}\big(\epsilon(P,t)\big) \\ P \in [A,\ B], & \bar{\epsilon}(P) = \dfrac{1}{\Delta t}\displaystyle\int_0^{\Delta t} \epsilon(P,t)\,dt \end{cases} \tag{16}$$

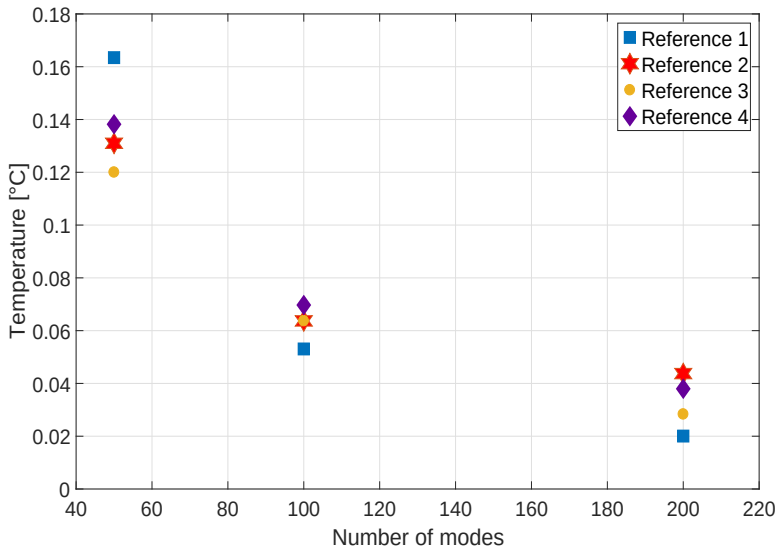

Figure 5: Maximum error at measuring points $\max\big(\epsilon_{max}(A),\ \epsilon_{max}(B)\big)$ for each reference cases

Figure 5 presents the maximum error between $\epsilon_{max}(A)$ and $\epsilon_{max}(B)$ (Eq.(16)) as a function of the order of the model. We note that according to the order of reduction chosen, the different reference cases do not have the same behaviour. Indeed the optimization of the reduced model (for a given $\tilde{n}$ order) is based on a global criterion (13) at the same time on the whole spatial and

temporal domain and for the 4 reference cases. It is therefore not possible to rigorously link this criterion to the punctual errors used thereafter.

We will then choose a model of order 100, which leads to a maximum error of less than 0.07[°C]. The temporal evolution of the temperature obtained by the complete and reduced models for the worst case scenario is shown in Figure 6. We can see that the maximum error is obtained during the first instants and it is evident that it will continue to decrease. Error related to the first instants is typical of model reduction, where the errors will be more related a priori to fast dynamics (high frequencies). As shown in Table 3, the mean error is largely lower regarding the maximum error at each measuring point.

Insulator	Point	ϵ_{max} [10^{-2} °C]	$\bar{\epsilon}$ [10^{-2} °C]	T_{max} [°C]
R1	A	5.31	1.61	31.50
	B	5.28	1.96	33.82
R2	A	6.37	0.76	15.82
	B	6.36	1.80	16.10
R3	A	5.50	2.55	7.90
	B	5.54	1.22	8.47
R4	A	6.97	2.04	4.54
	B	6.92	2.20	4.56

Table 3: Efficacy of the reduced order model of $\tilde{n} = 100$ modes of the reference cases

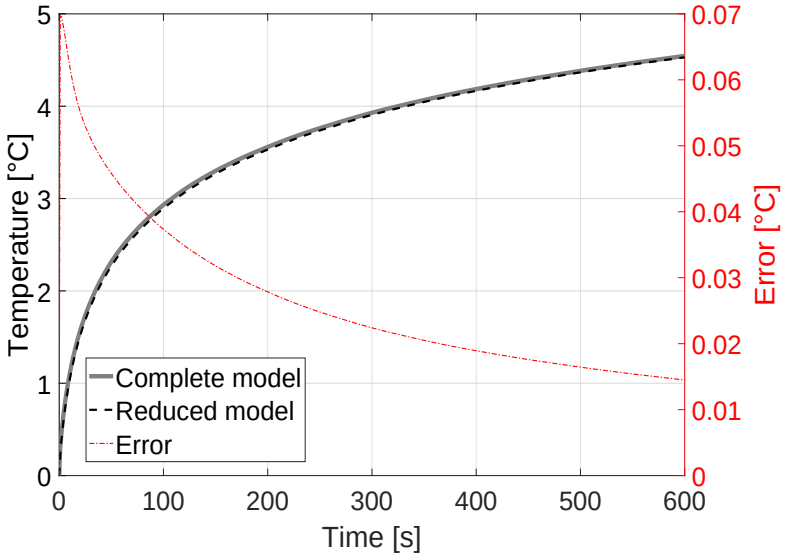

Figure 6: Reduced model of $\tilde{n} = 100$ modes : results for Reference n°4 at point A

3.4. State equation

The modal model is obtained by introducing the modal approximation of temperature (Eq.(5)) in the heat equation (Eq.(1)). Projecting the discrete heat equation (Eq.(3)) over this reduced basis by using the test function g as the basis eigenvectors:

$$\begin{aligned} \forall j \in \mathbb{N}, \quad & \sum_{i=1}^{\tilde{n}} \left(\int_{\Omega} \tilde{V}_j \, c \, \tilde{V}_i \, d\Omega \right) \frac{d\tilde{x}_i}{dt} \\ & = -\sum_{i=1}^{\tilde{n}} \left(\int_{\Omega} k \overrightarrow{\nabla} \tilde{V}_j . \overrightarrow{\nabla} \tilde{V}_i \, d\Omega + \int_{\Gamma} \tilde{V}_j \, h \, \tilde{V}_i \, d\Gamma \right) \tilde{x}_i \\ & + \int_{\Omega_{HW}} \tilde{V}_j \, \Pi \, d\Omega \end{aligned} \tag{17}$$

By making $\tilde{\mathbf{V}}$ the matrix grouping the entire $\tilde{n}$ of the reduced modes $\tilde{V}_i$ (expressed under a discrete form), and $\tilde{\mathbf{X}}$ being the vector of $\tilde{n}$ associated excitation states $\tilde{x}_i$, the reduced model equation corresponding to Eq.(4) is expressed as:

$$(c_I \widetilde{\mathbf{V}}^{\mathbf{t}} \mathbf{C_I} \widetilde{\mathbf{V}} + \widetilde{\mathbf{V}}^{\mathbf{t}} \mathbf{C_P} \widetilde{\mathbf{V}}) \dot{\widetilde{\mathbf{X}}} = (k_I \widetilde{\mathbf{V}}^{\mathbf{t}} \mathbf{K_I} \widetilde{\mathbf{V}} + \widetilde{\mathbf{V}}^{\mathbf{t}} \mathbf{A} \widetilde{\mathbf{V}}) \widetilde{\mathbf{X}} + \widetilde{\mathbf{V}}^{\mathbf{t}} \mathbf{U} \qquad (18)$$

that becomes under compact form:

$$(c_I \, \mathbf{L_I} + \mathbf{L_P}) \dot{\widetilde{\mathbf{X}}} = (k_I \, \mathbf{M_I} + \mathbf{M}) \widetilde{\mathbf{X}} + \mathbf{N} \qquad (19)$$

By solving this problem, it is possible to determine the transient evolution of the $\tilde{n}$ excitation states and also rebuild the temperature field $\tilde{T}(M,t)$ (Eq.(5)).

This simulation by reduced model is then used for 5 samples of insulating materials frequently used, which have different thermal properties (see Table 4) from those used to build the reduced model (see Table 2). We note that the range of thermal properties of these samples is significantly smaller regarding the wider range used for the reference cases. This choice was made with a view of conducting experimental validations.

The maximum errors at the two measurement points of these reduced simulations compared to the results obtained by the complete model are presented in Table 5. It is worth pointing out that the results present the same order of error as that obtained by projection for the reference materials (Table 2).

No. of sample	k_I [W.m^{-1}.K^{-1}]	c_I [J.m^{-3}.K^{-1}]
1	0.030	7.2×10^4
2	0.041	1.15×10^5
3	0.035	2.6×10^4
4	0.028	2.2×10^4
5	0.022	3.5×10^4

Table 4: Thermal properties of the tested insulators

These results show the capacity of these reduced models obtained by the AROMM method to be used for a wide range of the insulator's physical properties. In terms of computation time, the use of this reduced model ($\tilde{n} = 100$) compared to a classic finite element type model ($N \approx 62{,}000$), leads to a gain of 250 times faster. It is this result that justifies the use of this type of reduced model for an inverse process to identify parameters.

Sample	Point	$\epsilon_{max}\,[10^{-2}\ °\mathrm{C}]$	$\bar{\epsilon}\,[10^{-2}\ °\mathrm{C}]$	$T_{max}\,[°\mathrm{C}]$
S1	A	5.577	0.709	12.06
	B	5.541	0.691	12.31
S2	A	5.735	0.543	8.95
	B	5.696	0.847	9.05
S3	A	5.465	1.906	11.68
	B	5.465	0.527	12.16
S4	A	5.417	2.079	14.18
	B	5.413	0.724	14.83
S5	A	5.435	1.195	16.50
	B	5.409	1.025	17.12

Table 5: Reduced model of $\tilde{n} = 100$ modes : errors of the samples

4. Inverse procedure

4.1. Principle

From the temperature field obtained, by using an inverse technique, we are able to identify the thermal properties (k_I and c_I) of the targeted insulating material.

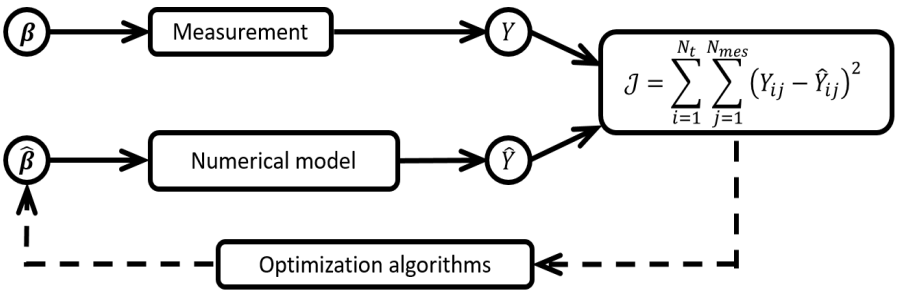

Figure 7: Inverse procedure scheme

Figure 7 demonstrates the iterative process aimed at identifying the best solution. In practice, the inverse approach focuses on N_{mes} specific points, through a selection matrix $\mathbf{E}$, that creates an observable vector $\widehat{\mathbf{Y}}$ to compute an approximation of $\widehat{\boldsymbol{\beta}} = [\widehat{k}_I, \widehat{c}_I]$.

The goal here is to replace the numerical model by a reduced order model previously built:

$$\widehat{\mathbf{Y}} = \mathbf{ET} \approx \mathbf{E}\tilde{\mathbf{V}}\tilde{\mathbf{X}} \tag{20}$$

The iterative identification process is based on the minimization of a quadratic criterion built on the difference between the measurement Y_{ij} at the measurement points and the result of the simulation $\widehat{Y}_{ij}$ for the estimated parameters $\widehat{\boldsymbol{\beta}}$ at each iteration. Here it is important to note that the measurements Y_{ij} are calculated with a complete model with added noise and the simulation $\widehat{Y}_{ij}$ is performed by the reduced model.

$$\mathcal{J}(\widehat{\boldsymbol{\beta}}) = \frac{1}{2} \sum_{i=1}^{N_t} \sum_{j=1}^{N_{mes}} \left(Y_{ij} - \widehat{Y}_{ij}(\widehat{\boldsymbol{\beta}}) \right)^2 \tag{21}$$

where N_t is the number of time steps of the simulation.

As for the optimization algorithm, a series of approaches can be implemented at different degrees of complexity in accordance with the sought parameters. This will be addressed in Section 4.3.

4.2. Sensitivity study

In order to assess the feasibility of the procedure to identify thermal properties, we conducted a sensitivity study to ensure the relevance of the measurements points, since the sensitivity to the variation of parameters is scaled. They were evaluated by using:

$$S^*_{k_I} = k_I \frac{\partial Y}{\partial k_I} \qquad\qquad S^*_{c_I} = c_I \frac{\partial Y}{\partial c_I} \tag{22}$$

This study focused on the wide range of thermal properties within the reference cases and on the more restrained range of thermal properties in the samples listed for future experimental studies.

First of all, in order to quantify the expected accuracy of this identification, the evolution of these sensitivities as a function of time is plotted. Regarding the reference cases, we noted on Figure 8 a remarkable difference in magnitude of the sensibility for each parameter according to the reference cases 1 and 4. Furthermore, both sensitivities for the heat capacity are considerably smaller than those for the conductivity. Even if the reduced model allows the reproduction of a wide range of materials by simulation, the identification could eventually pose a problem.

Figure 9 shows the results regarding the samples. The sensitivities are enclosed in inside the domain previously obtained by the reference cases, and their variation for the same parameter are closer. We noticed that the sensitivity in relation to the heat capacity is once again lower than that of the conductivity. Thus, we could expect less accurate results during the identification procedure.

Next, in order to study an eventual correlation between these two parameters, one traces them one in relation to the other. Figure 10 represents the evolution of the sensitivity of the capacity as a function of that of the conductivity. It is chosen here to adimentionnalize these values as a function of the maximum values obtained, in order to obtain the same scale for the two reference cases studied R1 and R4. It can thus be noted that none of these evolutions follows a linear law: there is no correlation between these

sensitivities and the simultaneous identification of thermal conductivity and heat capacity is therefore theoretically possible by this hot-wire method.

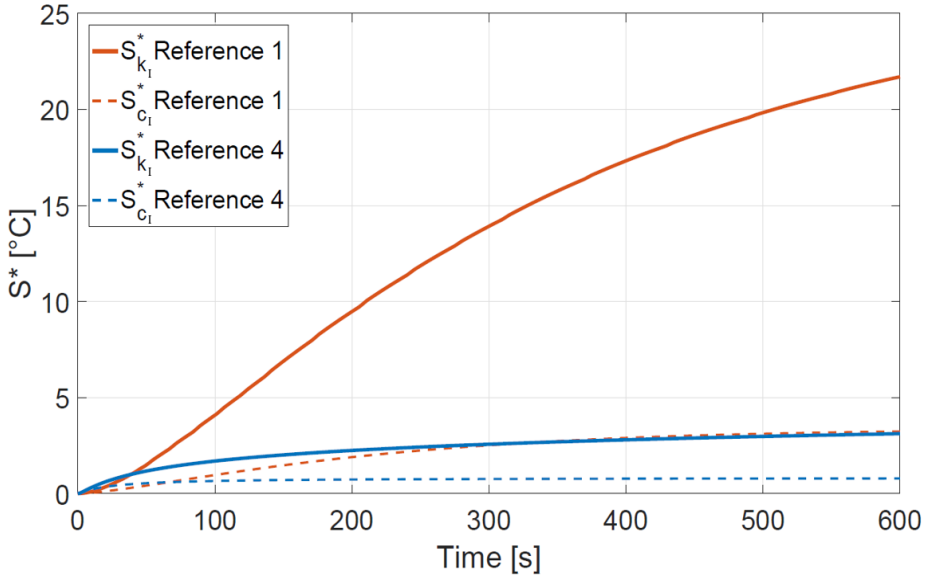

Figure 8: Sensitivity study for Reference R1 and R4

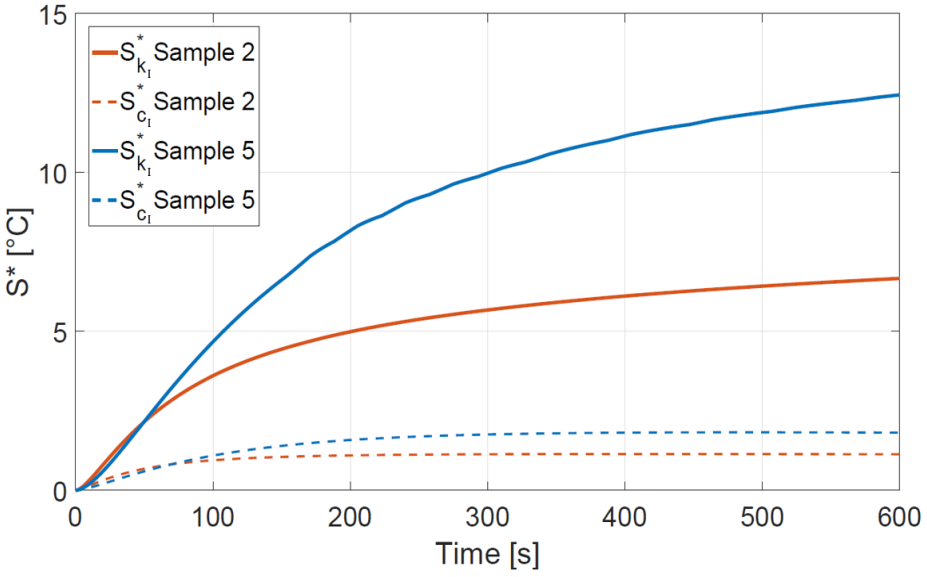

Figure 9: Sensitivity study for Sample S2 and S5

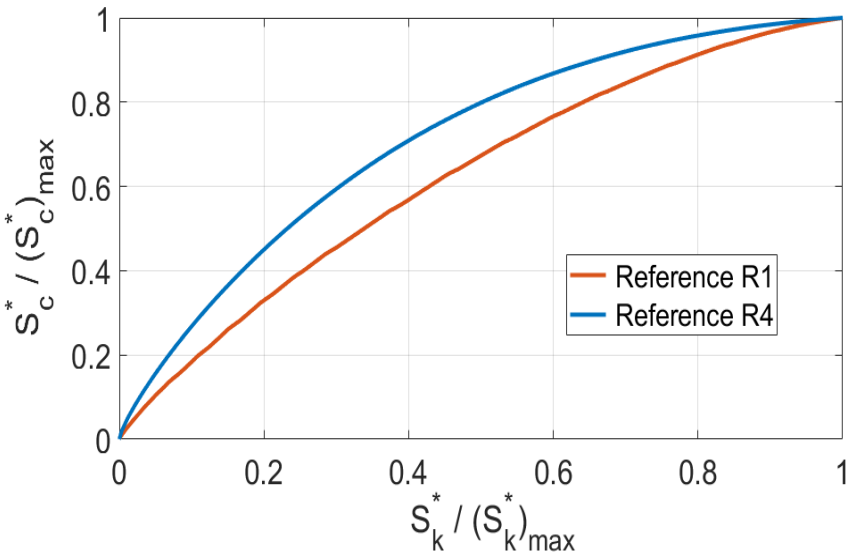

Figure 10: Correlation between the adimensionnalised sensivity for Reference R1 and R4

4.3. Minimization method

There are a variety of methods to carry out a function minimization. In this study we explored a stochastic method by the name of Particle Swarm Optimization, that is a population-based stochastic technique inspired by the social and cognitive behavior of a bird flock [47, 48].

Its principle is based on a random particle population that updates its positions and velocity at every iteration, looking to converge at the minimum of the specified function. In our case, being the thermal set of parameters the targeted value, the algorithm will update the thermal conductivity and capacity until a minimum is found (See annexe A for details).

The iterative process comes to an end when:

- the functional Eq.(21) stops evolving,
- the maximum number of iterations is achieved,
- the Morozov discrepancy principle is reached [49].

One can appreciate a series of captures of the PSO algorithm for Sample 1 in Figure 11. The first iteration allows to visualize the different initial values of the particle population, which are randomly chosen in the possible field of research of the parameters (k_I, c_I).

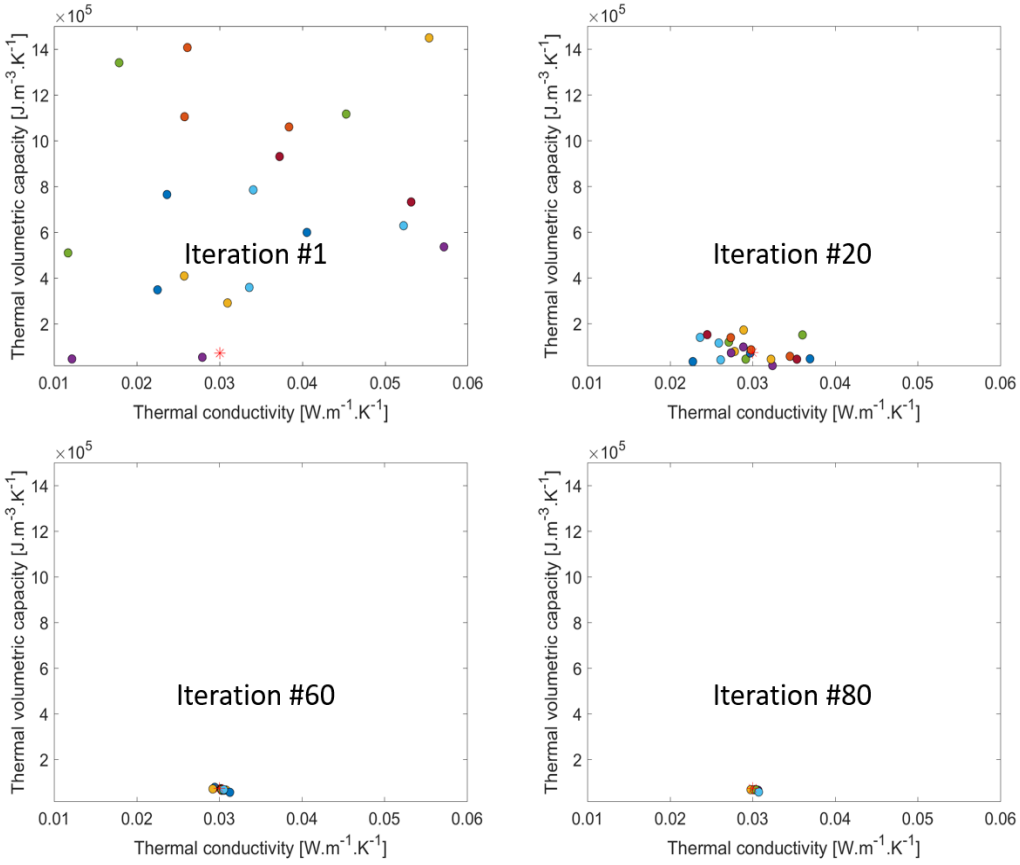

Figure 11: Particles evolution for PSO algorithm for sample No.1

4.4. Identification results

4.4.1. Identification without measurement noise

From virtual measurements obtained by numerical simulations carried out using a complete model (Eq.(4)), we are seeking the set of thermal characteristics of different materials. On the one hand, those who have been used for the construction of the reduced model (Table 2) and, on the other hand, those that are commonly used (Table 4).

For a given parameter β_i, we define σ_{β_i} as the relative error of the average value, and σ_{total} as the quadratic error between the measurement and the temperature built with the parameters identified:

$$\sigma_{\beta_i} = \frac{|\hat{\beta}_i - \beta_i|}{\beta_i} \tag{23}$$

$$\sigma_{total} = \sqrt{\frac{1}{2\ N_t\ N_{mes}} \sum_{i=1}^{N_t} \sum_{j=1}^{N_{mes}} \left(Y_{ij} - \widehat{Y}_{ij}(\widehat{\boldsymbol{\beta}}) \right)^2} \tag{24}$$

The set of results obtained with an absence of measurement noise is presented on Table 6.

	k_i	$\widehat{k}_I$	σ_{k_I}	c_i	$\widehat{c}_I$	σ_{c_I}	σ_{total}	t_{cpu}
	$[10^{-2}$ W.m^{-1}.K$^{-1}]$		[%]	$[10^4$ J.m^{-3}.K$^{-1}]$		[%]	[°C]	[s]
S1	3.000	3.011	0.4	7.200	6.868	4.6	0.016	220
S2	4.100	4.121	0.5	11.500	10.830	5.8	0.011	189
S3	3.500	3.464	1.0	2.600	2.713	4.4	0.015	192
S4	2.800	2.775	0.9	2.200	2.295	4.3	0.018	204
S5	2.200	2.199	0.1	3.500	2.199	1.5	0.021	198

Table 6: Identification without measurement noise

Regarding the reference materials (Ref.1 - Ref.4), the accuracy in the results is highly satisfactory since the overall of the identified parameters show an error under 1%, except for the heat capacity of Reference 4 sample, for which the error has an order of magnitude of 6%. This result is completely justified by the low sensitivity observed previously in Figure 8.

With regard to the conventional insulators (samples 1 to 5), it is noted that the identification errors are globally satisfactory. In terms of the thermal conductivity, identification error remains under 1%, whereas the error for the heat capacity reaches 6% at its maximum.

We note that the quadratic error σ_{total} corresponds to the error found between the reduced and complete model.

With respect to the calculations time, they are always under 5 minutes. The benefit of using a reduced model within this iterative procedure, which needs a large number of simulations, then becomes obvious. As an example, in the case of Sample 1, it took 200 iterations, and taking into consideration that the number of particles used in each iteration equals 20, this leads to

4,000 simulations. By using a simple extrapolation, an identification using a complete model will take approximately 20 hours of computation time.

4.4.2. Influence of a measurement noise

In this section we studied Sample 1 for which a stochastic noise with zero mean, and constant standard deviation $\sigma_{B_1} = 0.05[°C]$, and uncorrelated along time is added (Gaussian noise). In order to characterize the dispersion of the results linked to this noise, a large number of identifications are carried out ($n_I = 300$) which allows to evaluate for every identified magnitude β_i:

- the average value defined by:

$$\bar{\beta}_i = \frac{1}{n_I} \sum_{j=1}^{n_I} \hat{\beta}_i^j \tag{25}$$

- the standard deviation characterized by the dispersion of the estimation $\hat{\beta}_i^j$ of parameter β_i around the expectation of the estimator:

$$std_{\beta_i} = \sqrt{\frac{1}{n_I} \sum_{j=1}^{n_I} \left(\hat{\beta}_i^j - \bar{\beta}_i \right)^2} \tag{26}$$

- the average error:

$$\bar{\sigma}_{\beta_i} = |\bar{\beta}_i - \beta_i| \tag{27}$$

- the confidence interval corresponds to the maximum error made on one measurement with a probability of 99.7%:

$$\bar{\sigma}_{max} = \bar{\sigma}_{\beta_i} + 3 \; std_{\beta_i} \tag{28}$$

The results dispersion is illustrated in Figures 12 and 13, as well as in more detail in Table 7.

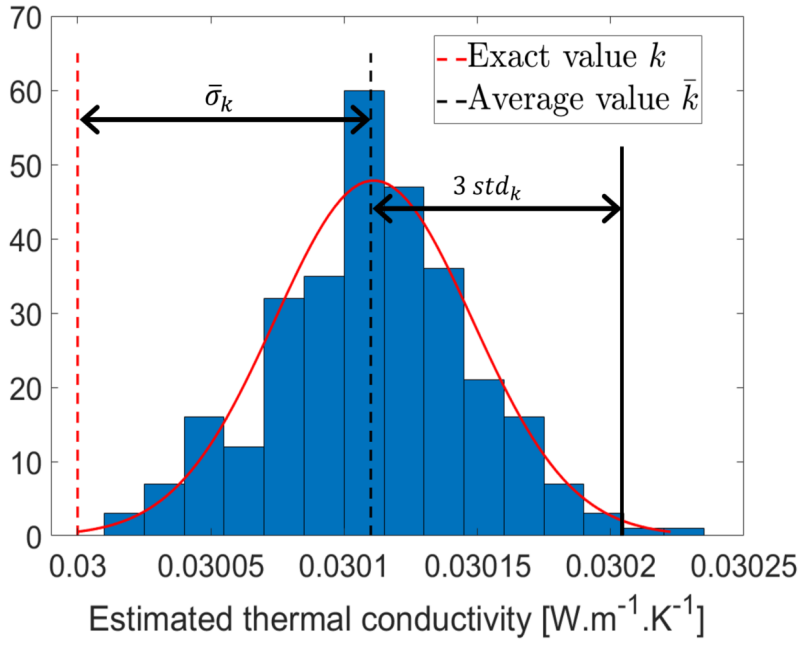

Figure 12: Identification of k for a $\sigma_B = 0.05°C$

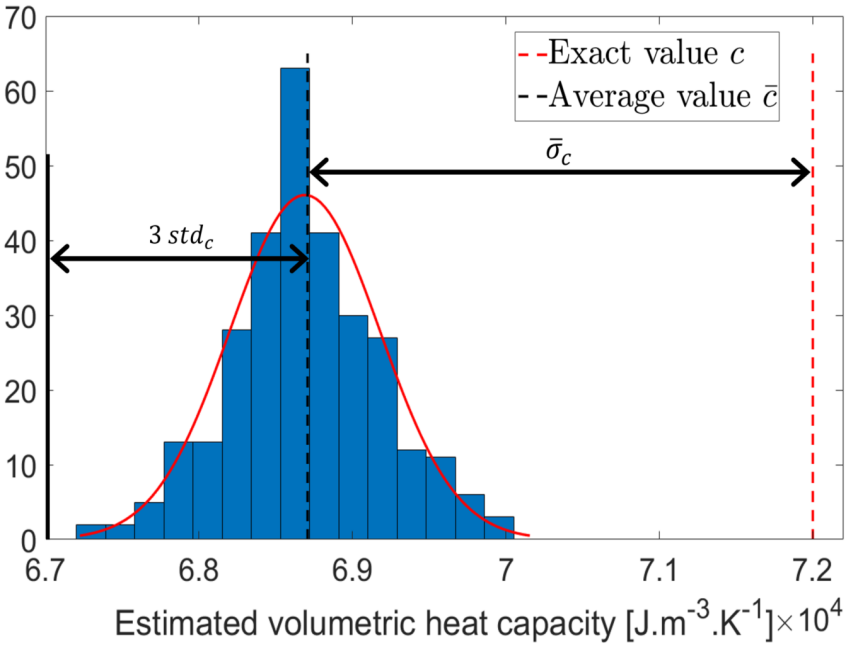

Figure 13: Identification of c for a $\sigma_B = 0.05°C$

β_i	k_I [10^{-2} W.m^{-1}.K^{-1}]	c_I [10^4 J.m^{-3}.K^{-1}]
Exact β_i	3	7.2
$\bar{\beta}_i$	3.011	6.871
std_{β_i}	0.004	0.059
$\bar{\sigma}_{\beta_i}$	0.011	0.329
σ_{max}	0.023	0.506

Table 7: Statistical study with measurement noise

At first we saw that each of the 300 identifications gave highly satisfying results. Secondly, for each parameter the average value $\bar{\beta}_i$ of these identifications corresponds exactly to the values obtained without measurement noise (see Table 6). Thus, the average error $\bar{\sigma}_{\beta_i}$ gives insight to the error between the complete and the reduced model. Moreover, the standard deviation std_{β_i} remains entirely reasonable compared to the real value β_i. The confidence interval σ_{max}, chosen voluntarily wide, gives 0.8% for the thermal conductivity and 7% for the heat capacity, respectively. The relative errors $\bar{\sigma}_{\beta_i}/\beta_i$ are 0.4% for the conductivity and 4.6% for the heat capacity.

It is possible to obtain theoretically standard deviation values without performing the 300 estimations. It depends on the sensitivities of the measurements at each point A and B, in relation to the parameter to be identified k_I and c_I, grouped together in the form of a sensitivity matrix:

$$\boldsymbol{S} = \left[\frac{\partial \boldsymbol{Y}}{\partial \beta_i}\right] \tag{29}$$

To quantify the quality of the estimation procedure, one can calculate the variance-covariance matrix defined by:

$$\boldsymbol{cov}\left(\hat{\boldsymbol{\beta}}\right) = \sigma_B^2 \left(\boldsymbol{S}^T \boldsymbol{S}\right)^{-1} \tag{30}$$

This covariance matrix has diagonal elements which enables us to approximate the theoretical standard deviation:

$$std_{\beta_i} \approx \sqrt{cov(i,i)} \tag{31}$$

In the case of Sample 1 we obtained:

Sample	std_k [10^{-2}W.m^{-1}.K^{-1}]	std_c[10^4J.m^{-3}.K^{-1}]
S1	0.004	0.050

These results are compared to those obtained from the 300 estimations shown on Table 7. In terms of the thermal conductivity, the approximation is accurate. As for the heat capacity, there is a difference of 20%, and one can appreciate that the standard deviation std_c remains smaller regarding the real value of the heat capacity c.

This technique is applied to approximate the confidence interval σ_{max} (Eq.(28)), since the average value $\overline{\sigma}_{\beta_i}$ corresponds to the value without noise (see Table 6). Table 8 regroups these estimations for all the samples for two different noises.

	Conductivity: $\sigma_{max_k}[\%]$		Heat capacity: $\sigma_{max_c}[\%]$	
Sample	$\sigma_B = 0.05[^\circ C]$	$\sigma_B = 0.1[^\circ C]$	$\sigma_B = 0.05[^\circ C]$	$\sigma_B = 0.1[^\circ C]$
S1	0.70	1.06	6.66	8.73
S2	0.96	1.44	8.70	11.31
S3	1.43	1.71	6.41	8.58
S4	1.32	1.57	5.98	7.87
S5	0.72	0.99	3.12	4.81

Table 8: Estimations of the confidence interval σ_{max} for different measurement noises σ_B

Overall results for these estimations are satisfactory. As noted before, the estimation of the heat capacity is less precise when compared to that of the conductivity. Moreover, a bigger measurement noise σ_B leads to a slight increase of the confidence interval σ_{max}.

One single estimation is conducted for each sample for both of the measurement noises. Table 9 presents the corresponding error, which remains within the confidence interval.

	Conductivity: $\sigma_k[\%]$		Heat capacity: $\sigma_c[\%]$	
Sample	$\sigma_B = 0.05[°C]$	$\sigma_B = 0.1[°C]$	$\sigma_B = 0.05[°C]$	$\sigma_B = 0.1[°C]$
S1	0.33	0.10	4.30	1.87
S2	0.40	0.78	5.38	7.28
S3	1.04	1.25	4.23	6.25
S4	0.91	0.64	4.47	2.17
S5	0.06	0.06	1.36	2.03

Table 9: One single identification for different measurement noises σ_B

4.5. Thermal contact resistance influence

In this section, we address the question of the presence of a thermal contact resistance (TCR) between the probe Ω_P and the insulating material Ω_I. In the reduced model used within the inverse procedure, this TCR was not taken into account, insofar as we consider that the probe is inserted in the insulator by breaking through the material, thus creating a perfect contact. However, in the literature, some authors refer to the existence of an imperfect contact between the probe and the material: Bording *et al* [30] analyzes the influence of TCR over a very broad spectrum (between 10^{-4} and $3\,[\mathrm{K.m^2.W^{-1}}]$) without experimental justification, and shows that TCR has little influence on the determination of the conductivity k but leads to errors on the capacity c. Two authors give TCR values depending on the material in which the probe is implanted: Wenlong *et al* [50] displays a TCR $\approx 10^{-3}[\mathrm{K.m^2.W^{-1}}]$ for ceramics. Goodhew *et al* [25] proposes values of TCR $= 5.10^{-3}[\mathrm{K.m^2.W^{-1}}]$ in clay straw and TCR $= 2.10^{-3}[\mathrm{K.m^2.W^{-1}}]$ in Agar. They do not specify the procedure for implanting the probe in the material (with or without pre-drilling before introduction of the probe).

In this study, we will evaluate the identification error when an TCR that appears in reality is not taken into account in the identification procedure.

The use of a numerical model which takes into account a contact resistance between the probe and the insulating material allows to obtain new virtual measurements from which the identification process is done with the previously reduced model (see Eq.(19)). This process is conducted without a measurement noise for the most sensitive sample S2 and for different values of TCR.

Table 10 shows the identification errors of the two parameters k_I and c_I

for different TCR values. The table specifies the correspondence in terms of equivalent air gap thickness around the probe, taking into account both the circular geometry of the probe and its very small size (The appendix presents the model used).

$TCR\,[10^{-3}\,\mathrm{K.m^2.W^{-1}}]$	e [mm]	σ_{k_I} [%]	σ_{c_I} [%]
0	0	0.51	5.83
0.25	0.015	0.76	9.13
0.50	0.03	0.62	11.82
1.00	0.03	0.39	16.71
1.64	0.10	0.73	22.54
5.00	0.34	2.14	44.98

Table 10: Influence de la TCR sur la precision de l'identification : materiau S2

We can thus see that we find the trends presented in the previous studies [30]:

On the one hand, the value of the identified thermal conductivity remains satisfactory whatever the quality of the contact between the probe and the air gap. Only a strong resistance ($TCR = 5\,10^{-3}\,[\mathrm{K.m^2.W^{-1}}]$) which corresponds to a pre-drilling a diameter significantly larger than the probe, leads to a significant error ($2\,[\%]$), of the same order of magnitude as the error related to the measurement noise (according to the table 8, an average measurement error of $0.1\,^oC$ leads to an identification error of $1.44\,\%$).

On the other hand, the results obtained show a very high sensitivity of the thermal capacity to the quality of the contact between the probe and the material. The difficulty to manage this parameter greatly degrades the quality of the identification of this capacity, which already depends significantly on measurement noise (the table 8 shows that an average measurement error of $0.1\,^oC$ leads to an identification error of about $11\,\%$).

This study brings to light the need of conducting a characterization for an imperfect contact between the probe and the material. In this case, the reduced model must then be adapted to take into account the estimated TCR.

5. Conclusion

This study evaluates the possibility of taking advantage of recent progress in reducing thermal models to extend the use of thermal characterization probes on site such as the hot-wire type. We wanted to be able to use them, on the one hand on strong insulating materials, which until now were difficult to characterize by this type of probes, and moreover to carry out a complete determination of the thermal properties, including the heat capacity.

This characterization requires a large numerical model to be able to perform a precise simulation taking into account the integrality of the thermal phenomena with the complex geometry of the probe. Given the incompatibility faced by large models in the face of an iterative process that constitutes the inverse problem posed, a solution is a reduced model, provided that the latter can be independent of the intrinsic properties of the model intended to be identified.

This study examined modal reduced models of the AROMM type. The advantage of these models is that they are built from complete families of eigenvectors, that form a base in H^1. These modal models are then independent of intrinsic parameters, such as the thermal conductivity and heat capacity. The construction of the reduced model was optimized from reference cases defining a wide range of insulating materials having a thermal conductivity varying from 1 to 6 [10^{-2} W.m^{-1}.K^{-1}] and, a thermal capacity value ranging from 1.5 to 150 [10^4 J.m^{-3}.K^{-1}]. Direct simulation tests for different materials with a single reduced model showed significant reduction in computation time (250 times) with a maximum error at the measurement points of less than 0.08 [$^\circ C$].

Therefore, the reduced model avoids a prohibitive computation time for an identification process. In order to estimate the influence of the reduced model within the inverse procedure, the first tests were carried out with virtual measurements obtained from a finite element complete model in the absence of noise. The results were highly satisfactory, even if it appeared that the low sensitivity of the temperatures measured with respect to the heat capacity generated an error reaching 6%.

A measurement noise study made it possible to show the feasibility of the method. The standard deviation, which is a function of the measurement noise, makes it possible to predict the confidence interval likely to be reached for a given probability. The tests conducted for all the materials examined had satisfactory results, with the worst case scenario resulting in 1.5% error

on thermal conductivity and 8.7% error on heat capacity, thus producing a total measurement noise of $\sigma_B = 0.05[^\circ C]$.

Furthermore, given the speed of the numerical calculations (< 5 min.) during the identification process, that employs a reduced model, one can imagine a continuous process of repeated identifications that overrides the influence of measurement noise, only to obtain an error solely related to the use of the reduced model.

Finally, the effect of an eventual imperfect contact between the probe and the insulating material was addressed by using virtual temperature measurements that took into account a given air gap. It was found that if there was thermal resistance, it could generate important additional errors for the heat capacity but acceptable for the thermal conductivity. Additional research will be required to assess this thermal resistance either by analyzing the state of the insulating material around the probe, or by identifying the resistance itself. The question then arises how to handle imperfect contact in the reduced model.

This study has shown the strength of reduced models to simulate complex thermal phenomena, always getting closer to reality.

This work was conducted for a real hot-wire type probe originally dedicated to the determination of the conductivity in an analytical way. This probe configuration is probably not optimal in terms of measurements sensitivity to the parameters to be identified, particularly to the heat capacity. Hence, the elaboration of a new probe configuration, which would allow greater sensitivity to heat capacity could generate better results. Regardless of the design of the probe, the use of the AROMM method in the inverse procedure would be efficient.

Finally, this technique could be extended to identify the same parameters for an orthotropic geometry, typical of thermal insulators, by implementing a new technological tool.

References

[1] ASTM, Standard Test Method for Steady-State Heat Flux Measurements and Thermal Transmission Properties by Means of the Guarded-Hot-Plate Apparatus, ASTM C117-19, Annual book of astm standards edition, 2000.

[2] Y. Jannot, A. Degiovanni, G. Payet, Thermal conductivity measurement of insulating materials with a three layers device, International Journal of Heat and Mass Transfer 52 (2009) 1105 – 1111.

[3] S. C. Nagpure, R. Dinwiddie, S. Babu, G. Rizzoni, B. Bhushan, T. Frech, Thermal diffusivity study of aged li-ion batteries using flash method, Journal of Power Sources 195 (2010) 872 – 876.

[4] M. Boutinguiza, F. Lusquiños, J. Pou, R. Soto, F. Quintero, R. Comesana, Thermal properties measurement of slate using laser flash method, Optics and Lasers in Engineering 50 (2012) 727 – 730.

[5] M. Akoshima, B. Hay, M. Neda, M. Grelard, Experimental verification to obtain intrinsic thermal diffusivity by laser-flash method, International Journal of Thermophysics 34 (2013) 778–791.

[6] P. Jeon, J. Kim, H. Kim, J. Yoo, Thermal conductivity measurement of anisotropic material using photothermal deflection method, Thermochimica Acta 477 (2008) 32–37.

[7] L. Pawlowski, P. Fauchais, The least square method in the determination of thermal diffusivity using a flash method, Revue de Physique Appliquee 21 (1986) 83–86.

[8] N. D. Milošević, M. Raynaud, K. D. Maglić, Simultaneous estimation of the thermal diffusivity and thermal contact resistance of thin solid films and coatings using the two-dimensional flash method, International Journal of Thermophysics 24 (2003) 799–819.

[9] J. Brouns, A. Crinière, J. Dumoulin, A. Nassiopoulos, F. Bourquin, Diagnostic de structures de génie civil : Identification des propriétés spatiales et de la surface d'un défaut, Congrès Société Française de Thermique (2014).

[10] P. Reulet, G. Leplat, Méthode inverse pour la détermination expérimentale des conductivités thermiques et de la capacité calorifique de matériaux orthotropes en fonction de la température, Congrès Société Française de Thermique (2011).

[11] W. Adamczyk, R. Bialecki, T. Kruczek, Retrieving thermal conductivities of isotropic and orthotropic materials, Applied Mathematical Modelling 40 (2016) 3410–3421.

[12] W. Adamczyk, Z. Ostrowki, Retrieving thermal conductivity of the solid sample using reduced order model inverse approach, International Journal of Numerical Methods for Heat & Fluid Flow 27 (2017) 729–739.

[13] H. Zhang, Y.-M. Li, W.-Q. Tao, Theoretical accuracy of anisotropic thermal conductivity determined by transient plane source method, International Journal of Heat and Mass Transfer 108 (2017) 1634 – 1644.

[14] S. Raji, Y. Jannot, P. Lagière, J.-R. Puiggali, Thermophysical characterization of a laminated solid-wood pine wall, Construction and Building Materials 23 (2009) 3189 – 3195.

[15] S. Lagüela, P. Bison, F. Peron, P. Romagnoni, Thermal conductivity measurements on wood materials with transient place source technique, Thermochimica Acta 600 (2015) 45 – 51.

[16] Y. Jannot, P. Meukam, Simplified estimation method for the determination of the thermal effusivity and thermal conductivity using a low cost hot strip, Measurement Science and Technology 15 (2004) 1932–1938.

[17] T. Kruczek, W. Adamczyk, R. Bialecki, In situ measurement of thermal diffusivity in anisotropic media, International Journal of Thermophysics 34 (2013) 467–485.

[18] E. El Rassy, Y. Billaud, D. Saury, Unconventional flash technique for the identification of multilayer thermal diffusivity tensors, International Journal of Thermal Sciences 155 (2020) 106430.

[19] J. Jaeger, Conduction of heat in an infinite region bounded internally by a circular cylinder of a perfect conductor, Australian Journal of Physics 9 (1956) 167 – 179.

[20] J. H. Blackwell, A transient flow method for determination of thermal constants of insulating materials in bulk part I - Theory, Journal of Applied Physics 25 (1954) 137–144.

[21] C. G. Pereira, J. V. Resende, G. G. Pereira, T. O. Giarola, M. E. Prado, Thermal conductivity measurements and predictive models for frozen guava and passion fruit pulps, International Journal of Food Properties 16 (2013) 778–789.

[22] H. Nahor, N. Scheerlinck, J. V. Impe, B. Nicolaï, Optimization of the temperature sensor position in a hot wire probe set up for estimation of the thermal properties of foods using optimal experimental design, Journal of Food Engineering 57 (2003) 103 – 110.

[23] N. I. Kömle, E. S. Hütter, W. Macher, E. Kaufmann, G. Kargl, J. Knollenberg, M. Grott, T. Spohn, R. Wawrzaszek, M. Banaszkiewicz, K. Seweryn, A. Hagermann, In situ methods for measuring thermal properties and heat flux on planetary bodies, Planetary and Space Science 59 (2011) 639 – 660.

[24] S. Nagihara, M. Hedlund, K. Zacny, P. Taylor, Improved data reduction algorithm for the needle probe method applied to in-situ thermal conductivity measurements of lunar and planetary regoliths, Planetary and Space Science 92 (2014) 49–56.

[25] S. Goodhew, R. Griffiths, Analysis of thermal-probe measurements using an iterative method to give sample conductivity and diffusivity data, Applied Energy 77 (2004) 205 – 223.

[26] W. Batty, S. Probert, M. Ball, P. O'Callaghan, Use of the thermal-probe technique for the measurement of the apparent thermal conductivities of moist materials, Applied Energy 18 (1984) 301 – 317.

[27] B. Pilkington, S. Grove, Thermal conductivity probe length to radius ratio problem when measuring building insulation materials, Construction and Building Materials 35 (2012) 531 – 546.

[28] H. Humaish, B. Ruet, L. Marmoret, H. Beji, Assessment of long time approximation equation to determine thermal conductivity of high porous materials with NSS probe, Journal of Sustainable Construction Materials and Technologies 1 (2016) 1–15.

[29] L. Marmoret, H. Humaish, Limit of validity of the log-linear model for determining thermal properties of light insulation materials with cylindrical hot probe, International Journal of Thermal Sciences 117 (2017) 251 – 259.

[30] T. S. Bording, S. B. Nielsen, N. Balling, Determination of thermal properties of materials by monte carlo inversion of pulsed needle probe data, International Journal of Heat and Mass Transfer 133 (2019) 154 – 165.

[31] Y. Rouizi, Y. Favennec, J. Ventura, D. Petit, Numerical model reduction of 2D steady incompressible laminar flows : Application on the flow over a backward-facing step, Journal of Computational Physics 228 (2009) 2239 – 2255.

[32] Y. Rouizi, M. Girault, Y. Favennec, D. Petit, Model reduction by the modal identification method in forced convection : Application to a heated flow over a backward-facing step, International Journal of Thermal Sciences 49 (2010) 1354 – 1368.

[33] D. González, F. Masson, F. Poulhaon, A. Leygue, E. Cueto, F. Chinesta, Proper generalized decomposition based dynamic data driven inverse identification, Mathematics and Computers in Simulation 82 (2012) 1677–1695.

[34] A. Fic, R. Bialecki, A. Kassab, Solving transient non linear heat conduction problems by proper orthogonal decomposition and the finite-element method, Numerical Heat Transfer, Part B: Fundamentals 48 (2005) 103–124.

[35] H. M. Park, O. Y. Chung, J. H. Lee, On the solution of inverse heat transfer problem using the karhunen loève galerkin method, International Journal of Heat and Mass Transfer 42 (1999) 127–142.

[36] A. Neveu, K. El-Khoury, B. Flament, Simulation de la conduction non linéaire en régime variable: décomposition sur les modes de branche, International Journal of Thermal Sciences 38 (1999) 289 – 304.

[37] E. Videcoq, O. Quéméner, M. Lazard, A. Neveu, Heat source identification and on-line temperature control by a branch eigenmodes reduced

model, International Journal of Heat and Mass Transfer 51 (2008) 4743 – 4752.

[38] E. Videcoq, M. Lazard, O. Quéméner, A. Neveu, Online temperature prediction using a branch eigenmode reduced model applied to cutting process, Numerical Heat Transfer, Part A: Applications 55 (2009) 683–705.

[39] S. Carmona, Y. Rouizi, O. Quéméner, F. Joly, A. Neveu, Estimation of heat flux by using reduced model and the adjoint method. application to a brake disc rotating, International Journal of Thermal Sciences 131 (2018) 94–104.

[40] S. Carmona, Y. Rouizi, O. Quéméner, Spatio-temporal identification of heat flux density using reduced models. application to a brake pad, International Journal of Heat and Mass Transfer 128 (2019) 1048 – 1063.

[41] W. P. Adamczyk, Z. Ostrowski, Retrieving thermal conductivity of the solid sample using reduced order model inverse approach, International Journal of Numerical Methods for Heat and Fluid Flow 27 (2017) 729–739.

[42] M. Girault, L. Cordier, E. Videcoq, Parametric low-order models in transient heat diffusion by MIM. estimation of thermal conductivity in a 2d slab, Journal of Physics: Conference Series 395 (2012) 012019.

[43] R. Lehoucq, D. Sorenson, C. Yang, Arpack User's Guide Solution of large scale eigenvalue problem with implicit restarted Arnoldi method, SIAM, Philadelphia PA, 1998.

[44] S. Marshall, An approximation method for reducing the order of linear system, Control (1966) 642–653.

[45] F. Joly, O. Quéméner, A. Neveu, Modal reduction of an advection-diffusion model using a branch basis, Numerical Heat Transfer, Part B: Fundamentals 53 (2008) 466–485.

[46] O. Quéméner, F. Joly, A. Neveu, The generalized amalgam method for modal reduction, International Journal of Heat and Mass Transfer 55 (2012) 1197 – 1207.

[47] M. Clerc, J. Kennedy, The particle swarm-explosion, stability, and convergence in a multidimensional complex space, IEEE Transactions on Evolutionary Computation 6 (2002) 58–73.

[48] M. Clerc, L'optimisation par essaim particulaire, Technique et Science Informatiques 21 (2002) 941–964.

[49] J. V. Beck, B. Blackwell, C. R. Saint-Clair, Inverse Heat Conduction: Ill-Posed Problems, Wiley-Interscience publication, Wiley, 1985.

[50] W. Cheng, R. Ma, K. Xie, N. Liu, Y. Huang, Simultaneous measurement of thermal properties by thermal probe using stochastic approximation method, Applied Energy 88 (2011) 1834 – 1840.

[51] R. C. Eberhart, Y. Shi, Comparing inertia weights and constriction factors in particle swarm optimization, Proceedings of the 2000 Congress on Evolutionary Computation 1 (2000) 84–88.

Annexe A : The PSO technique

Algorithm 1: PSO algorithm

```
Result: [k_I,c_I]
Rand Initialize position β for each particle;
Initialize velocity v = 0 for each particle;
while termination condition is not fullfilled do
    foreach particle do
        compute velocity v (Eq.32);
        compute position β (Eq.33);
        if position in feasible space then
            evaluate position;
        end
    end
end
```

$$v_i^{t+1} = \chi \; v_i^t + \lambda_1 \cdot rand^t(pBest_i^t - p_i^t) + \lambda_2 \cdot rand^t(gBest^t - p_i^t) \tag{32}$$

$$\boldsymbol{\beta}_i^{t+1} = \boldsymbol{\beta}_i^t + v_i^{t+1} \tag{33}$$

Eq.(32) allows to update the particle velocities. The first term concerns the inertia, it makes the particle move in the same direction and with the same velocity. The second term is linked to the personal influence, it improves the individual by making the particle return to a previous position better than the current one. And the third term regards the social influence, meaning that the particle will follow the best neighbors direction.

Eq.(33) moves each particle to their new position where:

- $\boldsymbol{\beta}$ represents the particle position,
- $\boldsymbol{v}$ the path direction,
- χ the weight of local information, also considered the inertia factor, it defines the exploration capacity of each particle,
- λ_1 and λ_2 are the weight of global information, also known as construction factors,
- pBest is the best position of the particle,
- gBest is the best position of the swarm,

– rand is a random number between [0,1]

For this study, the PSO parameters are as follows: number of particles $p = 20$, $\chi = 0.7298$ and $\lambda_1 = \lambda_2 = 1.46618$. These parameters were chosen in order to assure the convergence of the algorithm [51].

Annexe B : Correspondence between TCR and equivalent air gap

We consider here the case of a homogeneous probe that dissipates a power P uniformly distributed in the volume. Placed in a cylindrical material and neglecting the ends of the probe, the axial symmetry allows the use of two analytical models :

- the case of the air gap uniformly surrounding the probe is represented on Figure 14(a), and a simple power balance allows to write :

$$\varphi = \frac{T_1 - T_3}{\frac{ln\left(\frac{D+2e}{D}\right)}{2\pi L k_{air}} + \frac{ln\left(\frac{D_{tot}}{D+2e}\right)}{2\pi L k_I}} \tag{34}$$

- the case of an equivalent thermal resistance TCR which imposes a temperature jump at the interface between the probe and the insulation leads to (Figure 14(b)) :

$$\varphi = \frac{T_1 - T_3}{\frac{TCR}{\pi DL} + \frac{ln\left(\frac{D_{tot}}{D}\right)}{2\pi L k_I}} \tag{35}$$

The equality of the different resistances of the equations (34) and (35) gives:

$$\frac{ln\left(\frac{D+2e}{D}\right)}{2\pi L k_{air}} + \frac{ln\left(\frac{D_{tot}}{D+2e}\right)}{2\pi L k_I} = \frac{TCR}{\pi DL} + \frac{ln\left(\frac{D_{tot}}{D}\right)}{2\pi L k_I} = \frac{TCR}{\pi DL} + \frac{ln\left(\frac{D_{tot}}{D+2e}\right) + ln\left(\frac{D+2e}{D}\right)}{2\pi L k_I} \tag{36}$$

or finally

$$TCR = \frac{D}{2}\, ln\Big(\frac{D+2e}{D}\Big)\Big(\frac{1}{k_{air}} - \frac{1}{k_I}\Big) \tag{37}$$

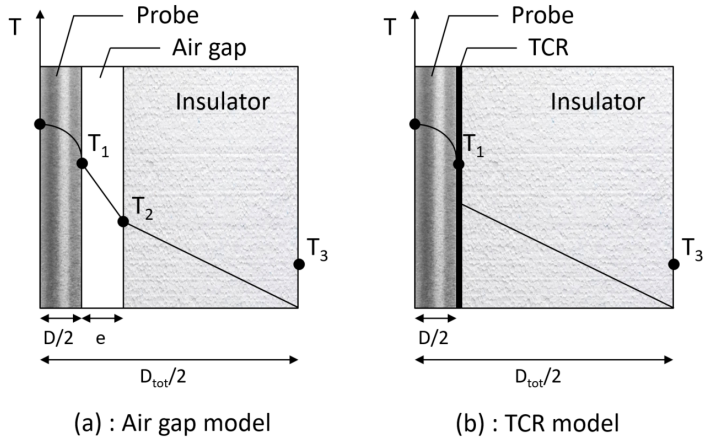

Figure 14: Contact Resistance Model Configurations

We can see here that the expression of the equivalent contact resistance is no longer as simple as the $TCR = e/k_{air}$ model used frequently. This contact resistance depends not only on the cylindrical geometry, but also on the conductivity of the material in which the probe is inserted.